

AERODYNAMIC STUDY OF HIGH-LIFT DEVICE CONFIGURATIONS FOR TAKE-OFF AND LANDING CONDITIONS

João Alves de O. Neto*, Carlos B. Júnior**, Darci Cavali,** and João Luiz F. Azevedo***

*Instituto Tecnológico de Aeronáutica, CTA/ITA/IEE,

**Universidade do Vale do Paraíba,

***Instituto de Aeronáutica e Espaço, CTA/IAE/ASA-L

Keywords: *High-lift Devices, CFD, Aerodynamic Coefficients, Turbulence Models*

Abstract

The purpose of the present paper is to perform a study of high-lift configurations using CFD simulations. Such study is an attempt to establish guidelines for the analysis and design of such devices through computational aerodynamics techniques. The study is motivated by the realization that an increased understanding of high-lift systems plays an important role in designing the next generation transport aircraft. Studies ranged from bibliography review of the most up to date known techniques for high-lift configurations analysis, 2-D simulations based on the steady state Euler equations coupled to the boundary layer equations and, finally, simulations of Reynolds-averaged Navier-Stokes codes for both 2-D and 3-D configurations.

1 Introduction

An increased understanding of high-lift systems will play an important role in designing the next generation of transport aircraft. Current designs for such aircraft typically involve multiple elements, such as leading edge slats and multiple-slotted flaps. The current trend is toward a more efficient, yet simpler design which will lead to reduced manufacturing and maintenance costs. At the same time, increases in lift coefficients for a given angle of attack and increases in maximum lift coefficient will lead to a larger payload capa-

bility. Increasing knowledge of the flow physics involved with high-lift systems is, therefore, of greater interest than ever before as the need to improve over current designs becomes acute.

Study of these configurations will require both computational and experimental efforts. Computational fluid dynamics (CFD) is playing a large role in such effort. Multi-element configurations present a number of challenging problems to the numerical investigations. These include problems involving turbulent boundary layer separation, confluent boundary layers and wakes, Reynolds number effects, three dimensional effects, compressible effects, transition and complex geometries. Although the problems are inherently three-dimensional, there is still much to be learned about the flow physics by studying two-dimensional models.

The computational tools available range from the more efficient and simpler inviscid/viscous coupled methods, to a Reynolds-averaged Navier-Stokes (RANS) analysis. An example of the former method is given by MSES code [1]. It is based on the solution of the Euler equations coupled with the boundary layer equations. These methods have been found to be successful in accurately computing the pressure distribution for the multi-element airfoils, including cases up to maximum lift, some of which involve separation. The coupled method has been proven to be useful as an effective engineering

design tool. Unfortunately, this method is limited by its inability to compute beyond maximum lift conditions, and it may have problems with certain features of some airfoil systems such as flap wells, thick trailing edges, or unsteady effects. The performance of high-lift configurations, especially close to stall, can be difficult to predict and requires the solution of at least the Reynolds-Averaged Navier-Stokes equations with an appropriate turbulence model. This is an expensive computational task which is made even more time consuming by the need of generating a field grid. The high-lift configurations are usually complex geometries, and at which complex flow physics are present.

Computational Fluid Dynamics (CFD) has been exhaustively used for aerodynamic design purposes due to the constant increase of the computational capabilities, the development and improvement of methodologies and the ease to obtain reliable results. The present paper uses the MSES and CFD++ [2] codes to simulate flows around high-lift aerodynamic configurations aiming at the prediction of lift, drag, moment and pressure coefficient distributions. In order to understand the flow physics over high-lift devices, three configurations are chosen for the studies to be performed in the present context. The multi-element airfoils selected were the NLR 7301 [3] and NHLP-2D [4] airfoils. Moreover, a 3-D configuration based on the RAE 1372 [5] profile was also selected. Such profiles were chosen based on availability of geometry and experimental data, for the flight conditions of interest for the present simulations, and also on the amount of published studies for the configurations.

2 High-Lift Configurations: Geometry and Grid Generation

Geometry of the 2D profiles was obtained in coordinate files and the trailing edges were not collapsed in neither elements. Mesh generation was performed with ANSYS ICEM CFD [6] and went through many parameters variations to check their influences on the final CFD result, such as farfield distance influence, bound-

ary layer and general refinement and mesh topology. Three geometries and flow conditions are considered in the present effort. These include a subsonic flow over a NLR 7301 airfoil, subsonic flow over a NHLP-2D airfoil and subsonic flow about a RAE 1372 configuration. The following test cases were considered:

- Simulations of subsonic flows about NLR 7301 airfoil. The simulation for this case is performed for Reynolds number $Re = 2.51 \times 10^6$ million and freestream Mach number $M_\infty = 0.185$. Numerical results are compared to available experimental results in order to assess the correctness of the validation. The mesh over the NLR 7301 profile is shown in Fig. 1. Both tri and quad meshes were generated for this configuration.

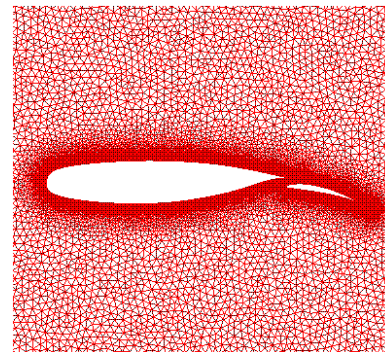


Fig. 1 Mesh over the NLR 7301 airfoil.

- Simulations of subsonic flows about NHLP-2D airfoil. The simulation for this case is performed for Reynolds number $Re = 3.52 \times 10^6$ million and freestream Mach number $M_\infty = 0.197$. Numerical results are compared to available experimental results in order to assess the correctness of the validation. The mesh over the NHLP-2D profile is shown in Fig. 2. Both tri and quad meshes were generated for this configuration.
- Simulations of subsonic flows about a RAE 1372 configuration [5]. The simulation for

AERODYNAMIC STUDY OF HIGH-LIFT DEVICE CONFIGURATIONS FOR TAKE-OFF AND LANDING CONDITIONS

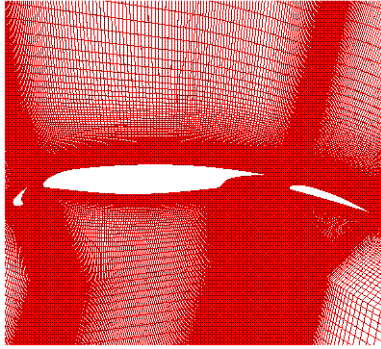


Fig. 2 Mesh over the NHLP-2D airfoil.

this case is performed for Reynolds number $Re = 1.35 \times 10^6$ million and freestream Mach number $M_\infty = 0.223$. Numerical results are considered in order to evaluate the correctness of the validation. The geometry of the profile was obtained from reference [5] along with the parameters to construct in a CAD environment the wing. Featuring a slat and flap double configuration, 31 degree of leading edge sweepback and high-lift devices over the whole span a tetrahedral mesh was generated with a total of 3.375.912 elements, in order to discretize the trailing edge of the elements, a well refined mesh was required. The mesh over the RAE 1372 configuration is shown in Fig. 3. In the computational study involving the cruise configuration. In the study, the fuselage and cruise wing were modeled. Once the RAE 1372 cruise configuration was obtained, started the mesh generation. Initially a tetra-prism based mesh was used for trials and initial setups. Later on hexa meshes might be used in order to improve mesh quality and robustness. The superficial and volumetric mesh was generated using ICEM CFD software.

An overall consideration on grid generation for high-lift design based on these analysis states that a hundred times the profile chord is the standard measure used on farfield distance. Boundary layer has a crucial importance in the final result and shall be discrete accordingly to the flow con-

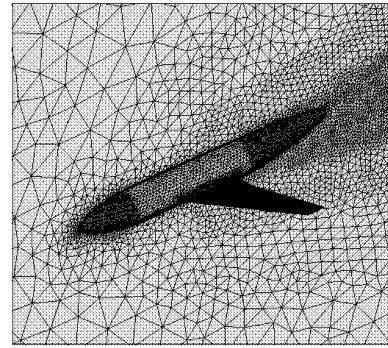


Fig. 3 Mesh over the RAE 1372 configuration.

ditions.

Once the boundary layer parameters are defined, a grid topology mesh may be created to better define the boundary layer limits. The hexa/quad mesh is the most indicated for high-lift CFD analysis but one must respect the topology orthogonally in order to preserve the mesh quality, based on the determinant of the elements which is the ratio of the smallest determinant of the Jacobian matrix divided by the largest determinant of the Jacobian matrix, where each determinant is computed at each node of the element. The determinant can be found for all linear hexahedral, quadrilateral, and pyramidal elements.

A consistent method for studying convergence of the computed solution with increasing grid density is an important pre-requisite for validating an automated CFD analysis procedure. Consistency of the grid system is difficult to achieve in analyzing high-lift flows. The difficulty arise out of the need to ensure sufficient grid density in regions of interesting flow phenomena while preventing deterioration of grid density and smoothness in other areas. The problem is further compounded by a lack of guideline regarding grid resolution requirements for the complex flow physics involving disparate length scales that arise in flowfields of multi-element high-lift configurations. The three principal areas of interest in the grid system are capture of the boundary layer effects, grid density on the geometry, and capture of wakes including regions of merging and separation of the freestream flow along boundary layer.

3 Flow Solution Method

3.1 Simulation Conditions

Usually, the solving step in the simulation process consumes most of the time. In order to know the number of simulations and flow conditions in this phase to dimension the time to dispend, it is indicated to have an estimation of expected results. In the early stages of the preliminary design of an airplane, some of the aerodynamic coefficients are already known due to a certain airplane performance that has to be achieved. In particular, the high-lift devices are intrinsically connected with the landing and the take-off performance. This two phases of the airplane mission are very important due to the operational implications that they have. An overestimated take-off C_l maximum implicates in limitations in the maximum weight to take-off, or the need for a longer track. In the same way, an overestimated landing C_l maximum implicates in the necessity for a longer track. The aerodynamic coefficients are directly influenced by the flow conditions (speed, altitude, temperature, etc), angle of attack and elements individual displacement parameters (gaps and overlaps). The designer must opt for the configuration where maximum lift coefficient is achieved, and to do so the number of simulations, combining all the cited parameters and conditions can grow out of limit on design time and costs to compute all the possible combinations. A solution must be addressed to reduce simulation time mainly.

3.2 MSES Code

The MSES code is a two dimensional analysis, design and optimization framework for multi-element airfoil sections. It is based on the steady state conservative Euler equations. The Euler equations are used to describe the inviscid part of the flow. The assumption that the viscous part is restricted to a thin boundary layer and wake is made, and the viscous part is described with the boundary layer theory given by the integrated Prandtl boundary layer equations [7]. The equations are discretized in an intrinsic grid,

where one set of coordinate lines correspond to the streamlines around the body. With this procedure the number of unknowns per grid node is reduced from four to two because the continuity equation and the energy equation can be replaced by the simple condition of constant mass flux and constant stagnation enthalpy along each stream-tube. The Newton method is used for solving the system of nonlinear equations. Simulations are performed quickly and the aerodynamic coefficients are obtained. A comparison of experimental data and the MSES code results are presented in the present paper.

3.3 CFD++ Code

The CFD++ code [2] allows easy treatment meshes of complex geometries mainly due to its integration of structured, unstructured and multi-blocks grids. Its flexibility allows the use of various elements within the same mesh such as hexahedral, triangular prism and tetrahedral elements in 3-D. However, as usual with RANS simulations for such high Reynolds number flows, the addition of turbulence models is required in order to capture the correct turbulent transport. In the present report, the use of both the Spalart-Allmaras (SA) one-equation and Menter SST (SST) two-equation models is foreseen. The codes to simulate flows around aerodynamic configurations aiming prediction of drag, lift and pressure coefficients to evaluate how codes is inserted in the main objective of this collaboration, and which consists in getting the aerodynamic coefficients as real as possible.

4 Results and Discussion

NLR 7301 Airfoil

The NLR 7301 is supercritical airfoil/flap configuration with 32% chord flap and considering a $\delta_f = 20^\circ$ flap deflection. In this present study, two different configurations are evaluated. The first analysis is performed for the configuration with a flap gap of 1.3% and the second one with the flap gap of 2.6%. In the present sim-

AERODYNAMIC STUDY OF HIGH-LIFT DEVICE CONFIGURATIONS FOR TAKE-OFF AND LANDING CONDITIONS

ulation, a triangular and quadrilaterals grid was used with 200.229 elements. The gap is defined as the radius of the circumference centered in the trailing edge of the main element and tangent to the flap profile in a certain point. This point of tangency is defined by the overhang, which is held at a constant at a value of 5.3% for both test cases here considered. It worth to mention that the gap and the overhang are defined as a percentage of the nominal profile cruise chord. The flap lower surface exhibited laminar flow at all times. The main element and flap boundary layers were found to be confluent for the flap gap of 1.3%. Simulations of subsonic flow over NLR 7301 profile were computed with freestream Mach number $M_\infty = 0.185$ and $Re = 2.51 \times 10^6$ million, using inviscid and viscous flow. In these simulations both Spalart-Allmaras (SA) and Menter SST (SST) turbulence models are exercised, as a form of comparing their results. In Fig. 4, one can observe the pressure contours over NLR 7301 airfoil obtained in the present calculations for the SA turbulence model.

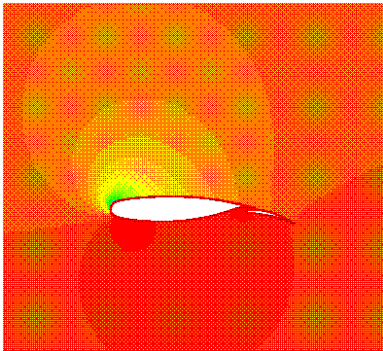


Fig. 4 Pressure coefficient using SA turbulence model for $\alpha = 13.1^\circ$ and $Re = 2.51 \times 10^6$ for the NLR 7301 airfoil.

The lift coefficient as a function of angle of attack can be observed in detail in Fig. 5. This figure compares SA, SST turbulence models and the MSES code with the experimental data. Comparison of experimental and calculated lift coefficients also show good agreement which is a clear indication of the good quality of the results that can be obtained with the CFD++ numerical tool.

One can observe in this figure that the numerical distributions compare very well with experimental data, less the MSES code. The relative worse agreement of predicted and experimental lift for the gap 1.3% may be attributed to a greater sensitivity of this case to the boundary layer development, which was not modeled correctly due to the laminar flow on the flap upper surface and relaminarization of the boundary layer in the flap cove region.

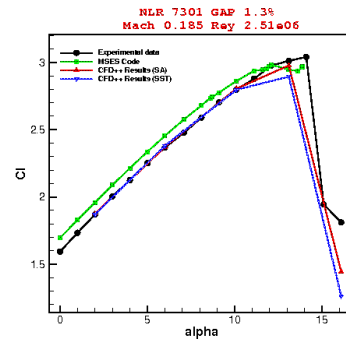


Fig. 5 The lift coefficient as a function of the angle of attack with Mach number 0.185 for NLR 7301 gap 1.3%.

The lift coefficient as a function of angle of attack can be observed in detail in Fig. 6 for NLR 7301 (2.6% gap). This figure compares SA, SST turbulence models and the MSES code with the experimental data. In Figs. 5 and 6, as in the NLR 7301 airfoil (1.3% and 2.6% gap) study the MSES results also present an overprediction of lift coefficient for this geometry. Due to the complexity of this simulated geometry, the differences in the lift coefficient as a function of angle of attack curve seem to have been more accentuated. For an perfect match with the experimental results, all the complex physics has to be perfectly capture. This includes the flow features at the cove of the main element, as well as the interactions between the free shear layer of the main element and the boundary layer of the flap. MSES code show a good capability to effectively reproduce the experimental data at the linear range. The limitations presented in the non-linear region are intrinsic to the MSES for-

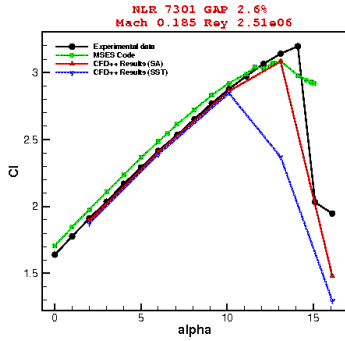


Fig. 6 The lift coefficient as a function of the angle of attack with Mach number 0.185 for NLR 7301 gap 2.6%.

mulation [8], as well the lack of a better control in relation to the mesh generation. This verification does not take the merits of the code since even other numerical codes with a formulation more adequate, Navier-Stokes an turbulence model, presents the same difficulty to present the aerodynamic coefficients with accuracy.

The experimental results are available [3]. The numerical pressure coefficient distribution shows an excellent agreement with the experimental data for the evaluated angles of attack. Figure 7 for flap gap 1.3% at an angle of attack of $\alpha = 6^\circ$, the comparison between the numerical and the experimental pressure coefficient distribution. In Fig. 8, one can observe the difference

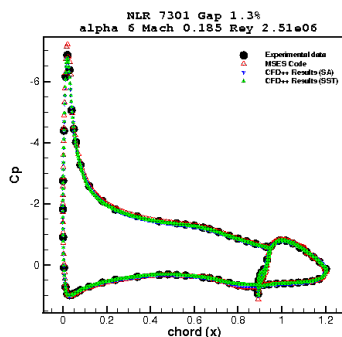


Fig. 7 The pressure coefficient as a function of the chord with $\alpha = 6^\circ$ for NLR 7301 gap 1.3%.

in the C_p distributions in the region of the cove. In Fig. 9, one can observe the comparison for an

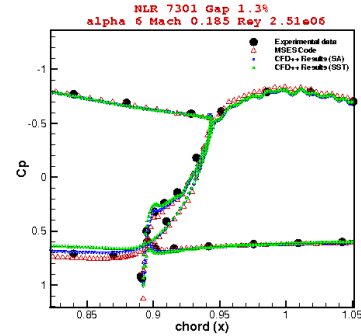


Fig. 8 C_p differences in the cove region with $\alpha = 6^\circ$ for NLR 7301 gap 1.3%

angle of attack of $\alpha = 13.1^\circ$. In Fig. 10, one can observe the difference in the C_p distributions in the region of the cove for $\alpha = 13.1^\circ$

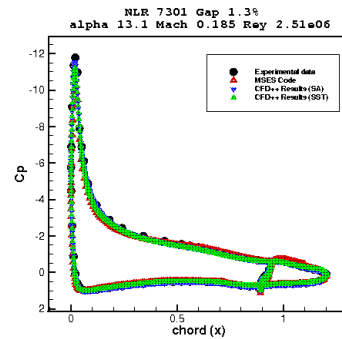


Fig. 9 The pressure coefficient as a function of the chord with $\alpha = 13.1^\circ$ for NLR 7301 gap 1.3%.

NHLP-2D Airfoil

The NHLP-2D airfoil is again a supercritical airfoil with a high-lift devices, including a 12.5% leading-edge slat and a 33% single-slotted flap [4]. For the results showed here, the slat and flap are deflected 25 and 20 deg., respectively, which is typical of take-off configurations with leading-edge stall. In the present simulation, a triangular and quadrilaterals mesh was used with 148014 elements. The NHLP-2D airfoil illustrated in Fig. 11 shows the flow over a typical high-lift airfoil with a leading edge slat and a single-slotted flap. The total pressure profiles as a function of chord

AERODYNAMIC STUDY OF HIGH-LIFT DEVICE CONFIGURATIONS FOR TAKE-OFF AND LANDING CONDITIONS

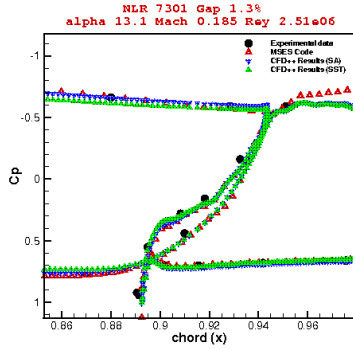


Fig. 10 C_p differences in the cove region with $\alpha = 13.1^\circ$ for NLR 7301 gap 1.3%

is shown in Fig. 12. The numerical results obtained by Morrison [9] using the Wilcox $k - \omega$ turbulence model are also presented together with experimental data [4].

The plot at $x/c = 0.35$ shows the slat wake and the boundary layer on the main element in the Fig. 13. The experimental data is more sparse in the region of the slat wake and shows a narrow and weak wake compared with the numerical results. The results of Morrison predict a slat wake too large. The plot at $x/c = 0.91$ and other downstream positions show the merging of the slat and main element wakes as described in Fig. 14. A distinct slat wake is predicted in the outer edge of the main element boundary layer all the way to the flap trailing edge in Fig. 15.

The pressure coefficient results are shown for the three elements for $\alpha = 4^\circ$ in Figs. 17, 18 and 19. The numerical results better compared with the experimental results at the main element and at the flap. It will be seen that the trailing-edge of the slats sits in the high-velocity region of the flow around the leading edge of the main wing. Because of this, the pressure coefficient at the trailing edge is significantly negative and thus the pressure rise on the slat is reduced. The same happens at the trailing-edge of the main wing due to the high velocities around the leading-edge of the highly deflected flap. In addition, the circulation around the slat induces a downwash on the main wing. This downwash clearly reduces with distance from the slat, so that it modifies the local

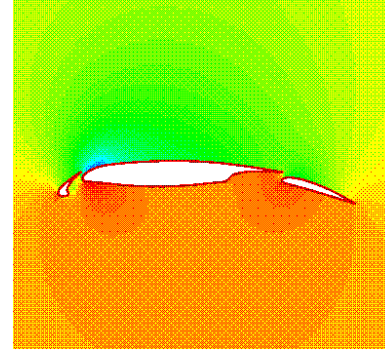


Fig. 11 Pressure contours using SA turbulence model for $\alpha = 4^\circ$ and $Re = 3.52 \times 10^6$ for the NHLP-2D airfoil.

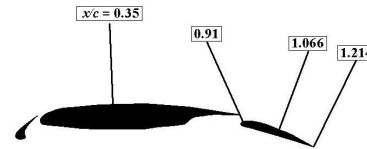


Fig. 12 Location of total pressure profiles for NHLP-2D airfoil.

velocities most strongly near the leading-edge of the wing, reducing it is peak suction markedly.

The same mechanism operates near the leading-edge of the flap. As a result of this, the pressure rise to the trailing-edge of the overall wing split up into a number of smaller pressure rises, when each of these is sufficient to just cause separation of the boundary layer, the overall pressure rise can clearly be very large.

RAE 1372 Configuration

A detail extremely important that verified it is that the results with wing-fuselage are merely qualitative. In fact, the configuration of the fuselage it is not given in details in the reference base, but the group did an approach judging to be interesting to analyze that case. Later, we will have quantitative results, because they will be just made simulations with the wing, disrespecting the fuselage. The Figs. 20 and 21 it shows pressure and mach contours for $\alpha = 0.05^\circ$, $M_\infty = 0.223$ and $Re = 1.35 \times 10^6$ such for the

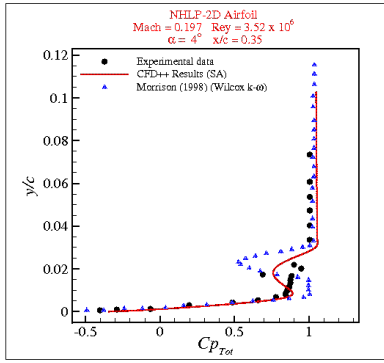


Fig. 13 Total pressure profile at $x/c = 0.35$.

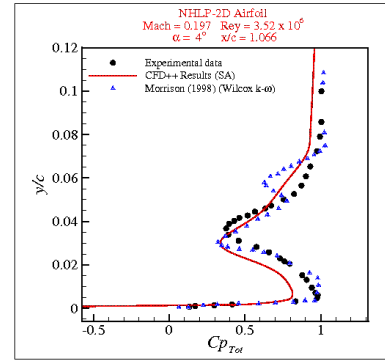


Fig. 15 Total pressure profile at $x/c = 1.066$.

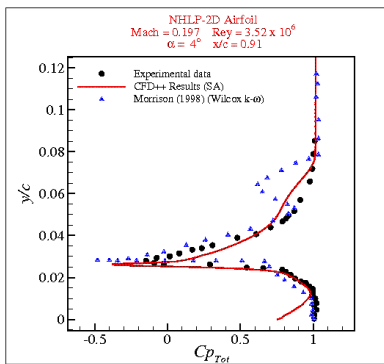


Fig. 14 Total pressure profile at $x/c = 0.91$.

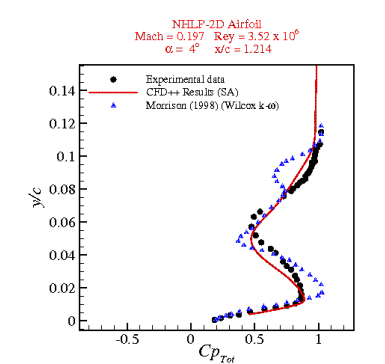


Fig. 16 Total pressure profile at $x/c = 1.214$.

Spalart-Allmaras turbulence model.

Table 1 Aerodynamic coefficients.

Aerodynamic Coefficients	C_L	C_D	C_M
Experimental Data	0.118	0.0092	-0.0528
Numerical Data	0.1123	0.007324	-0.05716

In Tab. 1, the results for the aerodynamic coefficients at $\alpha = 0.05$ deg. are presented. Although the results are rather preliminary, one can observe a fairly good agreement with the experimental data [5]. One should observe, however, that only qualitative comparisons are actually reasonable at this point due to the following reasons.

- The 3-D configuration, including fuselage and wing, is only an approximation of the real configuration and, therefore, the final result is affected.
- A large portion of the area of the fuselage is a cylinder, because the original reference [5] does not give the exact configuration. Hence, the authors have used the reported fuselage diameter in order to define a cylindrical fuselage. It is hoped that the use of the correct fuselage diameter at the wing-fuselage junction will minimize the errors so incurred.

5 Concluding Remarks

In the present paper, simulation results obtained with the SA and SST turbulence models are presented. Three geometries are considered in the present effort. These include a NLR 7301 air-

AERODYNAMIC STUDY OF HIGH-LIFT DEVICE CONFIGURATIONS FOR TAKE-OFF AND LANDING CONDITIONS

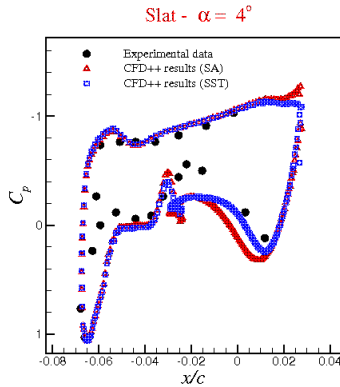


Fig. 17 Pressure coefficient at the slat for $\alpha = 4^\circ$ and $Re = 3.52 \times 10^6$ for the NHLP-2D airfoil.

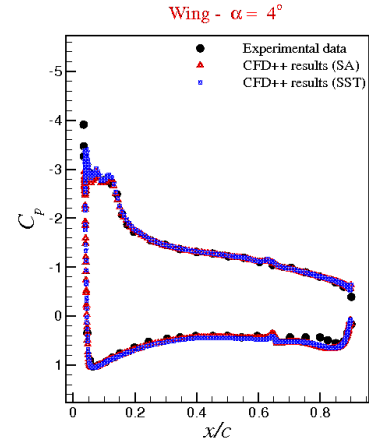


Fig. 18 Pressure coefficient at the wing for $\alpha = 4^\circ$ and $Re = 3.52 \times 10^6$ for the NHLP-2D airfoil.

foil, a NHLP-2D airfoil and an RAE 1372 airfoil-based wing configuration. The following test cases are considered:

- Simulations of subsonic flows about the NLR 7301 airfoil. The simulations for this case are performed for Reynolds number $Re = 2.51 \times 10^6$ and freestream Mach number $M_\infty = 0.185$. Numerical results are compared to available experimental data in order to assess the agreement obtained in this case.
- Simulations of subsonic flows about the NHLP-2D airfoil. The simulations for this case are performed for Reynolds number $Re = 3.52 \times 10^6$ and freestream Mach number $M_\infty = 0.197$. Numerical results are again compared to available experimental data.
- Simulations of subsonic flows about an RAE 1372 configuration, considering $Re = 1.35 \times 10^6$ and $M_\infty = 0.223$.

The paper provides a detailed comparison of the Spalart-Allmaras and Menter SST turbulence models in the context of two-dimensional high-lift aerodynamic flows. The results show that the Menter model is more accurate in separated flow regions. The SA model is more accurate in attached flows and wakes, including merging boundary layers and wakes. The SA model is

somewhat more robust, though for several cases the computational costs are about equal. Considering the uncertainties associated with the experimental data and the use of the RANS approximation, as well as the limitations on the grid resolution that can be used, the performance of these two turbulence models is excellent. They represent the state-of-the-art for this application. The SA model is preferred for general computations of aerodynamic flows, whereas the Menter model is the better choice if separated flows are of primary interest. A summary of the major conclusions of the study could be stated as follows:

- SA and SST models yielded generally similar results.
- Drag was sensitive to the farfield grid extent and/or to the boundary conditions.
- Grids larger than 90,000 elements were required for grid independence of drag, but lift and surface pressures were less grid sensitive.
- Not surprisingly, grid sizes tended to increase in density from less than 50,000 points to about triple such size as the decade advanced. Many independent grid studies seemed to suggest that 50,000 points may be sufficient to resolve surface pressures, but flow field quantities such as

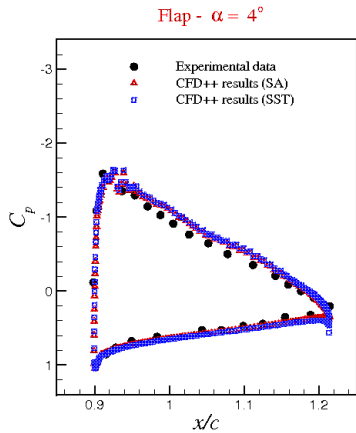


Fig. 19 Pressure coefficient at the flap for $\alpha = 4^\circ$ and $Re = 3.52 \times 10^6$ for the NHLP-2D airfoil.

velocity profiles require significantly more grid points. Some estimates indicate that, at least, 100.000 to 200.000 elements are required, unless a scheme with higher order spatial accuracy is employed. Grid issues tend to still remain very important in general. Those references that exercise the greatest care in ensuring high-quality, sufficiently refined grids with an accurate representation of the wind tunnel geometry tended to produce the best correlations with experiment. Underresolution in key areas, such as wakes, can lead to overdispersion and incorrect conclusions. Moreover, for 2-D computations, it is important to have a farfield grid extent of, at least, 50 to 60 chords or, otherwise, special farfield boundary condition treatment is required in order to accurately predict drag [10]. The inclusion of tunnel walls in the computations appears to be increasingly important at higher angles of attack.

- Grid distribution is also an important factor: sufficient grid resolution is required in key areas of the flowfield, *e.g.*, wakes and vortices.
- The configuration should be modeled as accurately as possible, *e.g.*, with the inclusion of support brackets, aeroelastic defor-

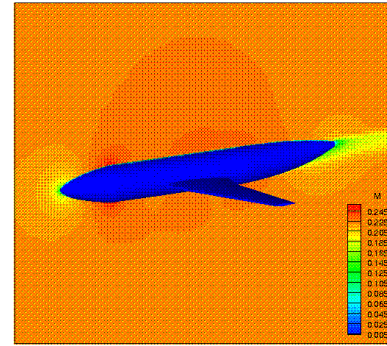


Fig. 20 Mach contours using SA turbulence model for $\alpha = 0.05^\circ$ and $Re = 1.35 \times 10^6$ for the RAE 1372 configuration.

mations, tunnel walls, chines), or otherwise these effects should be known. Geometry fidelity appears to be more crucial as the angle of attack approaches maximum lift.

- The fine grid was probably sufficiently fine for use at the lower angles of attack. However, its adequacy at higher angles of attack was dubious, particularly because of underresolution of the wall vortex.

Aside from the points listed above, some general conclusions from this work were: (a) 2-D CFD should not be expected to agree with the nominally 2-D wind tunnel experiment at high-lift conditions because the experiment loses its 2-D characteristics at high angles of attack, and (b) 3-D CFD using the current grids and methodology compared well with experiment at low angles of attack, but did not adequately model the character of the wind tunnel flow field near maximum lift. To improve this deficiency, based on the present experience, it is recommended that future 3-D CFD efforts include (in order of importance):

- Finer grid resolution in the region of the wall vortex, and overall finer resolution for unstructured grids;
- Top and bottom walls, and mounting brackets;

AERODYNAMIC STUDY OF HIGH-LIFT DEVICE CONFIGURATIONS FOR TAKE-OFF AND LANDING CONDITIONS

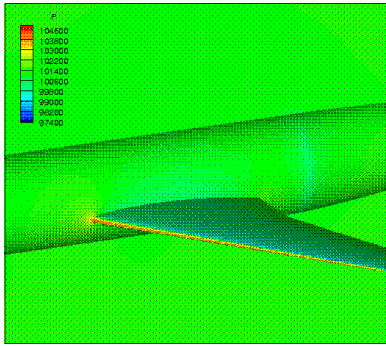


Fig. 21 Pressure contours using SA turbulence model for $\alpha = 0.05$ deg. and $Re = 1.35 \times 10^6$ for the RAE 1372 configuration.

- Better characterization of the incoming side-wall boundary layer.

6 Acknowledgments

The authors are indebted to Fundação de Amparo à Pesquisa do Estado de São Paulo, FAPESP, which provided support for the work through the Research Grant No. 2000/13768-4. The authors also acknowledge the partial support of Conselho Nacional de Desenvolvimento Científico e Tecnológico, CNPq, through the Integrated Project Research Grants No. 501200/2003-7 and 502053/2004-6.

7 References

- [1] Drela, M., “A User’s Guide to MSES 2.92”, MIT Computational Aerospace Sciences Laboratory, 1996.
- [2] “The CFD++ Computational Fluid Dynamics Software”, Metacomp Technologies, Inc., Westlake, CA, 2005.
- [3] Van den Berg, B., and Gooden, J.H.M., “Low-Speed Surface Pressure and Boundary Layer Measurement Data for the NLR 7301 Airfoil Section With Trailing Edge Flap”, *A Selection of Experimental Test Cases for the Validation of CFD Codes - AGARD AR-303*, vol. 2, pp. A9-1–A9-12, 1994.

- [4] Moir, I. R. M., “Measurements on a Two-Dimensional Aerofoil With High-Lift Devices”, *A Selection of Experimental Test Cases for the Validation of CFD Codes - AGARD-303*, vol. 2, pp. A2-1–A2-12, 1994.

- [5] Lovell, D. A., “A Wind-Tunnel Investigation of the Effects of Flap Span and Deflection Angle, Wing Planform and a Body on the High-Lift Performance of a 28° Swept Wing”, Aeronautical Research Council, ARC C.P. 1372, U.K., 1977.

- [6] “ANSYS ICEM CFD”, Reference Manual, ANSYS INC., 2005.

- [7] White, F. M., “*Viscous Fluid Flow*”, McGraw-Hill International Editions, Second edition, 1991.

- [8] Lima e Silva, A.L.F., Oliveira Neto, J. A., Antunes, A. P., Mendonça, M. T., Azevedo, J.L.F., and Silveira Neto, A., “Numerical Study of Two-Dimensional High-Lift Configurations Using the MSES Code”, *Proceedings of the 18th International Congress of Mechanical Engineering - COBEM 2005*, Ouro Preto, MG, Brazil, Nov. 2005.

- [9] Morrison, J. H., “Numerical Study of Turbulence Model Predictions for the MD 30P/30N and NHLP-2D Three-Element High-lift Configurations”, *NASA/CR-1998-208967*, 1998.

- [10] Basso, E., Azevedo, J.L.F., Bitencourt, L.O., and Andrade, T. J., “Cálculo do Escoamento Bidimensional sobre o Perfil RAE 2822 Utilizando o Software CFD++”, Relatório do IAE para o Núcleo de CFD, Instituto de Aeronáutica e Espaço, São José dos Campos, SP, Brazil, 2006.